Pattern Recognition 69 (2017) 199–212

Contents lists available at ScienceDirect

Pattern Recognition

journal homepage: www.elsevier.com/locate/patcog

Towards contactless palmprint recognition: A novel device, a new benchmark, and a collaborative representation based identification approach

Lin Zhang[a,b,*], Lida Li[a], Anqi Yang[a], Ying Shen[a], Meng Yang[c]

[a] School of Software Engineering, Tongji University, China
[b] Collaborative Innovation Center of Intelligent New Energy Vehicle, Tongji University, China
[c] School of Computer Science and Software Engineering, Shenzhen University, China

ARTICLE INFO

Article history:
Received 5 October 2016
Revised 10 March 2017
Accepted 15 April 2017
Available online 19 April 2017

Keywords:
Contactless palmprint recognition
Collaborative representation
Block-wise features
Image quality assessment

ABSTRACT

Biometric authentication has been found to be an effective method for recognizing a person's identity with a high confidence. In this field, the use of palmprint represents a recent trend. To make the palmprint-based recognition systems more user-friendly and sanitary, researchers have been investigating how to design such systems in a contactless manner. Though substantial effort has been devoted to this area, it is still not quite clear about the discriminant power of the contactless palmprint, mainly owing to lack of a public, large-scale, and high-quality benchmark dataset collected using a well-designed device. As an attempt to fill this gap, we have at first developed a highly user-friendly device for capturing high-quality contactless palmprint images. Then, with the developed device, a large-scale palmprint image dataset is established, comprising 12,000 images collected from 600 different palms in two separate sessions. To the best of our knowledge, it is the largest contactless palmprint image benchmark dataset ever collected. Besides, for the first time, the quality of collected images is analyzed using modern image quality assessment metrics. Furthermore, for contactless palmprint identification, we have proposed a novel approach, namely CR_CompCode, which can achieve high recognition accuracy while having an extremely low computational complexity. To make the results fully reproducible, the collected dataset and the related source codes are publicly available at http://sse.tongji.edu.cn/linzhang/contactlesspalm/index.htm.

1. Introduction

The need for reliable user authentication techniques has significantly increased in the wake of heightened concerns about security in networking, communication, and mobility [1]. Bolstered by the requirements of numerous applications, such as access control, aviation security, and e-banking, automatically recognizing the identity of a person with high confidence has become a topic of intense study. To address such an issue, biometric-based methods, which use unique physical or behavioral characteristics of human beings, have recently been drawing increasing attention because of their high accuracy and robustness. Actually, in the past decades or so, researchers have exhaustively investigated a number of different biometric identifiers, such as fingerprints [2,3], faces [4–7], irises [8–11], palmprints [12–16], hand geometry [17], fingerknuckle-print [18–20], ear [21], etc.

Among the many biometric identifiers, the palmprint has recently received significant attention due to its non-intrusiveness and ease of data collection. Palmprint refers to the skin patterns on the inner palm surface, comprising mainly two kinds of features, the palmar friction ridges (the ridge and valley structures like the fingerprint) and the palmar flexion creases (discontinuities in the epidermal ridge patterns) [13]. As an important member of the biometrics family, the palmprint is appealing and has various of desired properties, such as high distinctiveness, robustness, and high user-friendliness, etc. Actually, the use of palmprints for personal authentication can trace back to Chinese deeds of sale in the 16th century [22].

The first automated palmprint identification system became available in the early 1950s [13]. Since then, researchers have devoted a great deal of efforts in improving the effectiveness and efficiency of palmprint recognition systems. Currently, most devices for capturing palmprint images are contact-based (for example, the 2D palmprint acquisition device proposed in [12] and the 3D

* Corresponding author at: School of Software Engineering, Tongji University, China.
E-mail address: cslinzhang@tongji.edu.cn (L. Zhang).

http://dx.doi.org/10.1016/j.patcog.2017.04.016
0031-3203/

palmprint acquisition device proposed in [16]), which implies that the user needs to touch the device when his/her palmprint images are collected. When capturing palmprint images with contact-based devices, users are asked to put their hands on a planar surface and/or have fingers restricted by pegs. Obviously, such devices have their inherent drawbacks. At first, they are not user-friendly since the pose of user's hand needs to be strictly constrained when the image is captured [23]. Elderly or people with arthritis or other diseases that limit dexterity may have difficulty placing their hands on a flat surface (even guided by pegs) [24]. Secondly, the palmprint remains left by former users on the sensor's surface will possibly affect the image content or image quality of later users. That will probably decrease the system's accuracy. Moreover, those remained prints could be copied for illegitimate purposes [24,25]. Thirdly, when such a device is deployed in a case with a large number of users, it will raise hygienic concerns; people are concerned about placing their fingers or hands on the same sensor where countless others have also placed theirs [23,25]. Considering these shortcomings, recently, researchers have begun investigating how to build palmprint recognition systems in a contactless manner, which is also our focus in this paper.

The remainder of this paper is organized as follows. Section 2 introduces related work and our contributions. Section 3 introduces our newly designed contactless palmprint acquisition device. Our ROI extraction scheme is presented in Section 4. Section 5 presents our novel approach for contactless palmprint identification. Section 6 presents our newly established benchmark dataset and reports the experimental results. Finally, Section 7 concludes the paper.

2. Related work and our contributions

In this section, we will at first review some representative work in the field of contactless palmprint recognition from three aspects, the equipments designed for capturing contactless palmprint images, the collected benchmark datasets, and the matching methods. It needs to be noted that strictly speaking, the mobile palmprint recognition (i.e., performing palmprint recognition on mobile phones) also belongs to the field of contactless palmprint recognition. However, since that field has its own inherent characteristics and needs to be separately investigated, it will not be discussed in this paper.

2.1. Contactless palmprint acquisition devices

In [26], Chen et al. adopted a digital camera to acquire palmprint images against a dark background. In their system, two 3U 23-watt lights were used to provide illumination and were arranged in appropriate positions. Chen et al.'s setup is shown in Fig. 1(a), from which it can be seen that various hardware parts were not integrated into a complete usable system. In addition, with such a system, images can only be manually captured. Consequently, Chen et al.'s system can only be used in lab.

In Kumar's palmprint acquisition device [27], the camera, the lens, and the fluorescent light source are enclosed in a semi-closed box. For sample acquisition, the user can put his/her hand into the box inside, and then the palmprint image can be captured against a dark background (the top cover of the box). We cannot get any further information about this device since the author did not provide drawings or photos of its internal structure. From sample images captured, it can be seen that in Kumar's device [27] the free space left for the hand in the box is quite limited and thus it is highly likely that the user's fingers may touch the walls of the box. So, it may raise users' hygienic concerns. In Fig. 1(b), a sample image collected by Kumar's device is shown.

In [28], Hao et al. built a multispectral contactless palmprint recognition system, whose design is shown in Fig. 1(c). With Hao et al.'s system, when sample images are being captured, 6 groups of LEDs ranging from violet to near infrared (IR) will be switched on sequentially, and thus 6 images under different lighting conditions can be collected. It is easy to know that the data acquisition using such a device is quite time-consuming.

In [25,29], Michael et al. built a low-cost contactless palmprint acquisition device as shown in Fig. 1(d). A 1.3 mega pixel web camera and a 9W white light bulb are mounted inside a semi-closed box. As shown in Fig. 1(d), there is no top cover with Michael et al.'s device, which may cause two problems. At first, since the distance between the user's palm and the camera cannot be restricted, the quality of collected images may vary much. Secondly, when it works, its intense light may directly enter into the user's eyes, which will inevitably make the user uncomfortable. Therefore, this prototype system is maybe difficult to be commercialized.

In [30], Poinsot et al. collected palmprint images using a Logitech QuickCam Pro 9000 webcam against a green background. Neither a housing nor additional lights are used in their setup. Images are captured under natural illumination. One sample image collected by Poinsot et al. is shown in Fig. 1(e). Obviously, such a system cannot be used in practical security-critical applications.

In [31], Ferrer et al. proposed a bi-spectral contactless hand based biometric system, which could capture palm images under visible and IR lighting conditions simultaneously. The IR image is mainly used to facilitate the segmentation of the visible image. As shown in Fig. 1(f), Ferrer et al.'s device has no housing so it has similar potential problems as Michael et al.'s [25,29].

In order to study multi-sampling hand recognition, Morales et al. constructed a contactless palmprint acquisition device [32] as shown in Fig. 1(g). The design principle of this system is inspired by credit card readers. As shown in Fig. 1(g), two plates delimit the area through which the user passes his/her hand with a vertical movement. During the transit of the hand between two plates, sample images can be captured. With respect to the camera, Morales et al. adopted a Logitech C600 webcam.

Quite recently, Aykut and Ekinci developed a prototype system for contactless palmprint authentication [33], as shown in Fig. 1(h). Their capturing device is a low-cost CCD camera with a DC-auto iris lens. Using such a device, the distance between the user's hand and the camera cannot be restricted, so some captured images may be out of focus. In addition, since there are no back and forth walls of the device's housing, the LED light may hurt the user's eyes.

Main features and potential shortcomings of the existing contactless palmprint acquisition devices abovementioned are summarized in Table 1, following a chronological order. Having identified the disadvantages of the existing devices, it motivates us to design a novel one with the following characteristics. (1) All the hardware parts are enclosed in a housing. (2) The light source cannot hurt the user's eyes. (3) Enough space is reserved for the user to move his/her hand freely. (4) The distance between the camera and the user's hand is constrained to make sure the palm is within the camera's depth of field. (5) The collected image can have a simple dark background. Details of our novel contactless palmprint acquisition device can be found in Section 3.

2.2. Benchmark datasets publicly available

With the developed devices, some researchers have collected benchmark contactless palmprint datasets and made them publicly available.

In [28], Hao et al. collected a multispectral palm image dataset (CASIA dataset [34]). Images were taken from 200 hands in 2 separate sessions. In each session, there were 3 samples. Each

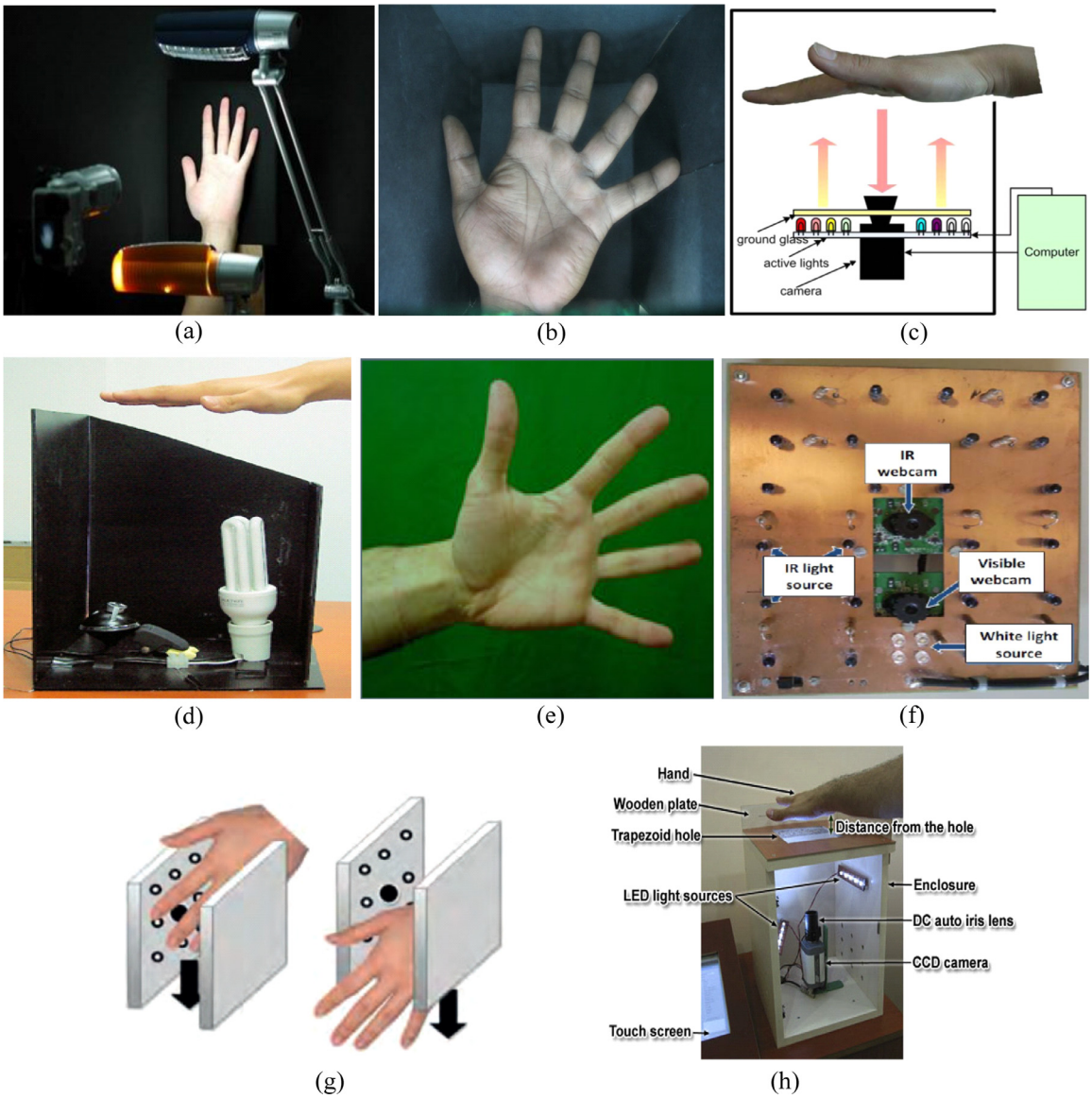

Fig. 1. (a) The palmprint acquisition device developed in [26]; (b) a sample image collected in [27]; (c) the multi-spectral palmprint acquisition device developed in [28]; (d) the palmprint acquisition device developed in [25,29]; (e) a sample image collected in [30]; (f) the palmprint acquisition device developed in [31]; (g) the palmprint acquisition device developed in [32]; (h) the palmprint acquisition device developed in [33].

sample includes 6 palm images captured under 6 different spectrums, 460 nm, 630 nm, 700 nm, 850 nm, 940 nm, and white light, respectively. So, there are altogether 7200 ($200 \times 2 \times 3 \times 6$) palm images in Hao et al.'s dataset. Among them, 4800 images are palmprint images (those taken under visible spectrums) and the other 2400 ones are palm vein images (those taken under IR spectrums). Using the self-developed device, Kumar collected a contactless palmprint dataset (referred as IIT dataset [35]), in which images were captured from 460 palms in a single session. Altogether, there are 2601 images in IIT dataset. Ferrer et al. have released a contactless palmprint dataset, referred as GPDS100 dataset [36]. Palmprint images in GPDS100 dataset were acquired from 100 palms within a single session. 10 images were acquired from each palm and thus the whole GPDS100 dataset contains 1000 sample images. The dataset collected by Aykut and Ekinci is referred as KTU dataset [37], comprising 1752 images collected from 145 different palms in a single session. In Section 6.1, information of these publicly available datasets along with our newly established dataset is summarized in Table 4.

2.3. Matching methods

In the field of contact-based palmprint recognition, coding-based methods have been demonstrated to be effective and efficient, such as PalmCode [12], CompCode [38], RLOC [39], OLOF (Orthogonal Line Ordinal Feature) [40], and they are actually inspired by the great success of Daugman's IrisCode [8] which was proposed for iris recognition. Some researchers have adapted these conventional coding-based recognition methods for contactless palmprint recognition. For example, PalmCode is used in [30,41], and OLOF [40] is used in [27,28,31,32].

Having been testified in various different applications, SIFT (Scale Invariant Feature Transform) [42] is an eminent method to extract image features in a scale-invariant way and it has also been exploited in the context of contactless palmprint recognition. In [43,44], when computing the similarity between two contactless palmprint images, Morales et al. fused the matching scores obtained by matching their SIFT features and by matching their OLOFs. Such a method is referred as "SIFT+OLOF" in this paper.

Table 1
Summary of existing contactless palmprint acquisition devices in the literature.

Refs.	Year	Main features	Shortcomings
Chen et al. [26]	2007	Two 3U 23-watt lights were used to provide illumination and were arranged in appropriate positions; a normal digital camera was used to capture the image.	Hardware parts were not integrated into a complete usable system; images can only be manually captured; it can only be used in lab.
Kumar [27]	2008	Hardware parts are enclosed in a semi-closed box; the palmprint image can be captured against a dark background.	The free space left for the hand in the box is quite limited and thus it is highly likely that the user's fingers may touch the walls of the box. So, it may raise users' hygienic concerns.
Hao et al. [28]	2008	It is a multispectral system; when sample images are being captured, 6 groups of LEDs will be switched on sequentially, and thus 6 images can be collected.	Palmprint acquisition using such a device is quite time-consuming; the light may hurt the user's eyes.
Michael et al. [25]	2008	A 1.3 mega pixel web camera and a 9W white light bulb are mounted inside a semi-closed box.	There is no top cover; the quality of collected images may vary much; when it works, its intense light may directly enter into the user's eyes.
Poinsot et al. [30]	2009	It collects palmprint images using a Logitech QuickCam Pro-9000 webcam against a green background under natural illumination.	Neither a housing nor additional lights are used in their setup; it cannot be deployed in practical applications.
Ferrer et al. [31]	2011	It could capture palm images under visible and IR lighting conditions simultaneously.	It has no housing so it has similar potential problems as Michael et al.'s [25].
Morales et al. [32]	2012	Two plates delimit the area through which the user passes his/her hand with a vertical movement.	The moving speed of the user's hand cannot be controlled so the quality of collected images may vary greatly.
Aykut et al. [33]	2015	Their capturing device is a low-cost CCD camera with a DC-auto iris lens.	The distance between the user's hand and the camera cannot be restricted, so captured images may be out of focus; the LED light may hurt the user's eyes.

In [45], to deal with the potential misalignment between two palmprint ROIs, Zhao et al. at first aligned the ROIs based on their matched SIFT feature points and then extracted CompCodes [38] from aligned ROIs. The final matching score is the fusion of the SIFT matching score and the CompCode matching score. Zhao et al.'s method [45] is referred as "SIFT+AlignedCompCode" in this paper. In Wu et al.'s scheme [23], an iterative RANSAC (Random Sampling Consensus) algorithm is at first employed to remove the mis-matched points and then local palmprint descriptors are extracted for SIFT points to further remove the mismatched points which cannot be correctly figured out by original SIFT descriptors. The number of final matched SIFT points is taken as the score for decision. In Wu et al.'s latest work [46], to solve the palmprint deformation problems, an iterative M-estimator sample consensus algorithm based on SIFT features is devised to compute piecewise-linear transformations to approximate the non-linear deformations of palmprints, and then stable regions are decided using a block growing algorithm. Palmprint feature extraction and matching are performed over the stable regions.

In Michael et al.'s contactless palmprint verification scheme [25], the feature vector is obtained by applying the LBP (Local Binary Pattern) operator on the image's directional gradient responses. For matching two such feature vectors, χ^2 distance is adopted as the dissimilarity metric. This approach is referred as "LBP+χ^2" in our paper. In [33,47], Ekinci and Aykut proposed a palmprint verification algorithm with the use of kernel Fisher discriminant analysis (KFD) [48] on the Gabor wavelet representations of palm images. Each palmprint sample is finally represented as a feature vector. To match two such feature vectors, the weighted Euclidean distance is used.

2.4. Our motivations and contributions

Having investigated the literature, we find that in the field of contactless palmprint recognition, there is still large room for further improvement in at least three aspects.

At first, for a biometric system, the design of the sample acquisition device is of profound importance. An ideal device needs to be highly user-friendly and the acquired images should be of high quality. Moreover, it is also anticipated that the collected image can have a simple background, which can greatly simplify the processing afterwards. However, these design principles are not well reflected in existing contactless palmprint acquisition devices.

Secondly, benchmark datasets are indispensable for researchers to devise more sophisticated recognition algorithms. An outstanding benchmark dataset is expected to comprise many classes and a large number of samples, collected from at least two separate sessions. Unfortunately, such datasets are still lacking for contactless palmprints.

Thirdly, though a plethora of techniques have been proposed for palmprint matching, nearly all of them are designed for one-to-one verification applications. When these methods are used to solve the one-to-many identification problem, to figure out the identity of a given test sample, it would be necessary to match the test sample to all the samples in the gallery set one by one. Such a brute-force matching strategy is obviously not quite computationally efficient, especially when the size of the gallery set is extremely large. Hence, how to solve the contactless palmprint identification problem efficiently still requires further efforts.

In this work, our aim is to thoroughly investigate the discriminant power of the contactless palmprint and to this end, we attempt to fill the abovementioned research gaps to some extent. Our contributions in this paper are summarized as follows:

(1) We have designed and developed a novel device for capturing contactless palmprint images. Our device has the following merits: it is highly user-friendly; the acquired images are of high quality; and the acquired image has a simple background.
(2) Using the developed device, we have established a large-scale contactless palmprint dataset and will make it publicly available to the research community. Our dataset is larger in scale than all the existing benchmark datasets for contactless palmprints. Besides, the image quality of our dataset is better than that of other datasets. Actually, a large-scale benchmark dataset with high quality images is crucial for exploring the discriminant capability of the contactless palmprint.
(3) To tackle the problem of large-scale contactless palmprint identification, we have proposed a collaborative representation (CR) [49] based scheme, namely CR_CompCode. CR_CompCode is the first work attempting to make use of CR-based classification schemes for contactless palmprint

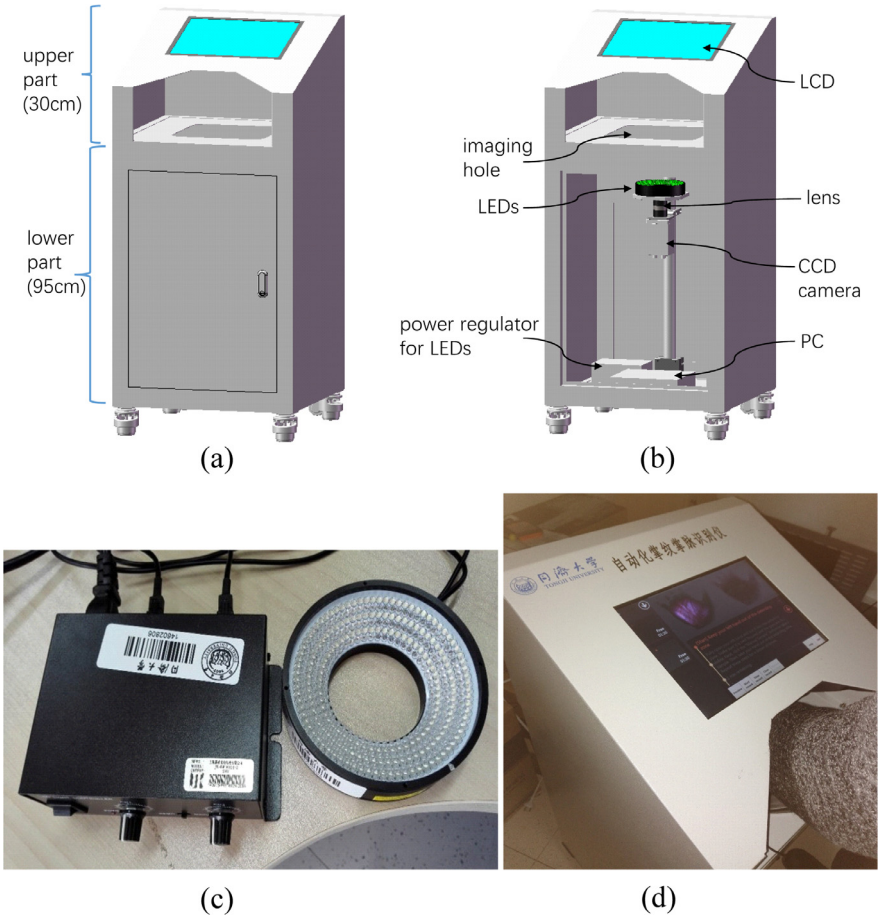

Fig. 2. (a) is the complete 3D CAD model of our contactless palmprint acquisition device while (b) shows its internal structure. (c) shows the lighting source and its power modulator used in our device. (d) One user is using the device. Our device is highly user-friendly: 1) all LEDs are enclosed in the housing, preventing them from hurting the user's eyes; 2) an LCD is mounted on the top cover, from which the user can observe the camera's video stream in real time; 3) the height of our device is about 950 mm, which is quite suitable for most adults; 4) enough space is reserved for the user to move his/her hand conveniently.

identification. Its superiority over the competing methods has been corroborated in experiments. To make results reproducible, the collected dataset and related source codes are publicly available at http://sse.tongji.edu.cn/linzhang/contactlesspalm/index.htm.

3. Contactless palmprint acquisition device

In order to investigate the discriminant capability of the contactless palmprint, we have at first devised and developed a novel contactless palmprint acquisition device, whose complete 3D CAD model is shown in Fig. 2(a). Its internal structure can be clearly observed from the 3D model shown in Fig. 2(b). Fig. 2(c) shows the lighting source and its power modulator used in our device. Fig. 2(d) shows a photo of our device being used by a subject. The device's metal housing comprises two parts. Its lower part encloses a CCD camera (JAI AD-80 GE), a lens, a ring light source composed of white LEDs, a power regulator for the light source, and an industrial computer. There is a square "imaging hole" on the top cover of the housing's lower part, whose center is on the optical axis of the lens. The size of the hole is 230 mm $\times$ 230 mm. The housing's upper part is wedge-shaped, on which a thin LCD with a touch screen is mounted. The height of our device is about 950mm and can be comfortably used by a normal adult. For data acquisition, the user needs to present his/her hand above the "imaging hole". The user can move his/her hand up and down freely within the space bounded by the housing's upper part and he/she can observe in real-time the camera's video stream from the LCD to adjust the hand's pose. The brightness of LEDs can be modulated by the power modulator. We carefully adjusted the position and the brightness of the LEDs to make the quality of collected images as high as possible.

Our newly developed device has the following characteristics. At first, as it is of high user friendliness, the user will feel comfortable when using it. The whole design is in accordance with ergonomics and we pay much attention to details. For example, all LEDs are enclosed in the housing, preventing them from hurting the user's eyes. Moreover, an LCD is mounted on the top cover, from which the user can observe the camera's video stream in real time. That can guide the user to adjust the hand pose and also can help alleviate the user's anxiety when using our equipment. Furthermore, the height of our device is about 950mm, which is quite suitable for most adults. Secondly, as we carefully adjusted the configurations of the camera, the lens, and the light source, the acquired images are of high quality, meaning that they have high contrast and high signal-to-noise ratio. Moreover, as the distance between the camera and the user's palm is restricted by the housing's upper part, the user's palm is always within the camera's depth of field. Four sample palmprint images collected using our device are shown in Fig. 3, from which it can be seen that even minute creases on the palmprints can be observed. Thirdly, with our device, the collected palmprint image can have a simple dark background because it is acquired against the dark back of the LCD. A simple background can largely reduce the complexity of the data processing afterwards and accordingly can improve the system's robustness.

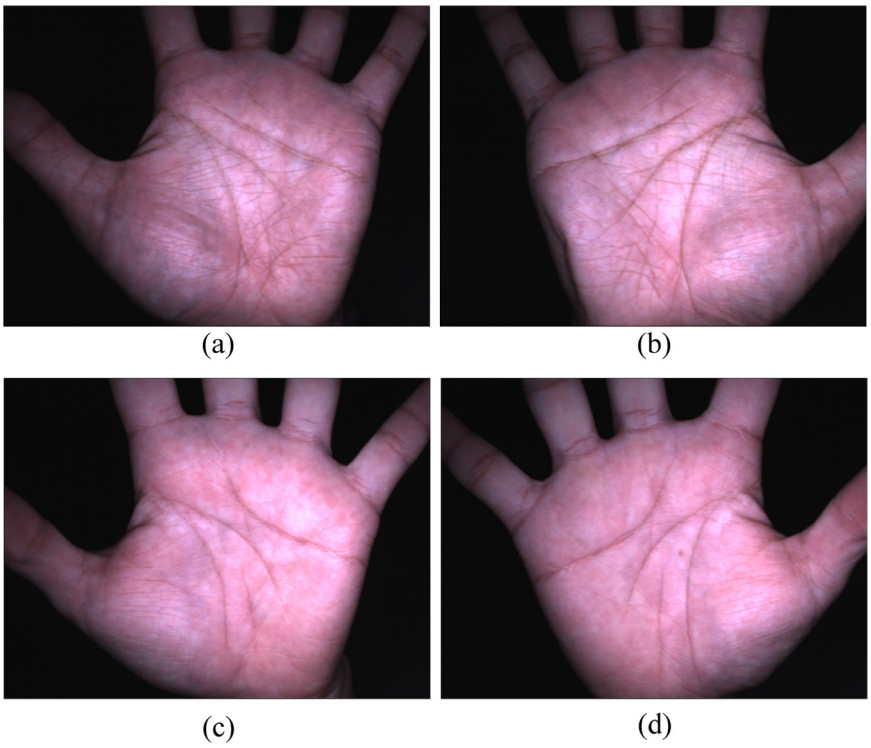

Fig. 3. (a) ~ (d) are four contactless palmprint images collected using our device.

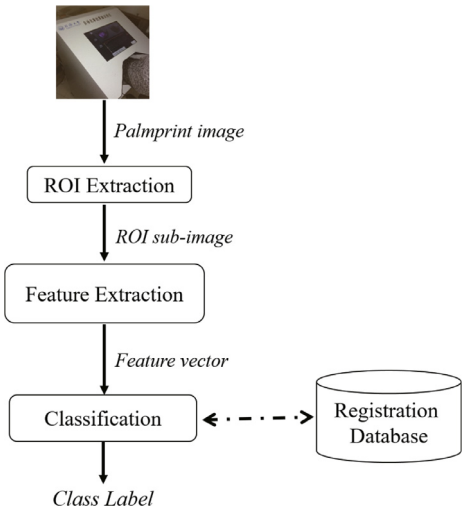

Fig. 4. The overall flowchart of our contactless palmprint identification system.

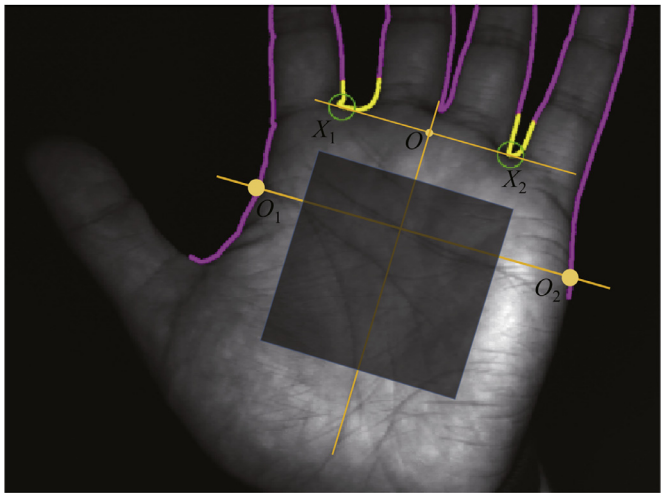

Fig. 5. Illustration for the proposed ROI extraction approach.

Using the developed device, we have established a large-scale contactless palmprint image dataset. Details can be found in Section 6.1.

4. ROI extraction

The pipeline of our contactless palmprint identification system is shown in Fig. 4. It can be seen that when the palmprint image is ready, three major steps are followed, ROI (region of interest) extraction, feature extraction, and classification. Our schemes for feature extraction and classification will be presented in Section 5. In this section, ROI extraction is introduced. In the pipeline of palmprint recognition, ROI extraction is the first influential step. Since global geometric transformations exist between two palmprint images, it is necessary and critical to align palmprint images by adaptively constructing a local coordinate system for each image. With such a coordinate system, an ROI can be cropped from the original image. The later feature extraction and matching are actually performed on ROIs. Our ROI extraction algorithm is motivated by Zhang et al.'s idea [12], which was originally proposed for contact-based palmprint images. It is highly desired that a contactless palmprint ROI extraction algorithm could be robust to translation, rotation, and scale variations of palmprints.

Given a palmprint image, we at first filter it using a low-pass filter, and then convert it to a binary image. Based on the binary palm mask, boundaries of two finger gaps (the gap between the index and the middle fingers and the gap between the ring and the little fingers) can be obtained. Then, we compute the tangent line of the two gap boundaries and denote the two tangent points by X_1 and X_2. The line passing through X_1 and X_2 is taken as the X-axis of the local coordinate system. The midpoint of X_1 and X_2

Table 2
The algorithm of ROI extraction from a contactless palmprint image.

Input: A palmprint image **I**.
Output: The ROI sub-image **R** extracted from **I**.
1. Low-pass filter **I** using a Gaussian filter and then convert it to a binary image **B**;
2. From **B**, extract boundaries of two finger gaps (as illustrated in Fig. 5);
3. Get the tangent line of the gap boundaries and the tangent points are X_1 and X_2;
4. $\overline{X_1X_2}$ is taken as the X-axis and the midpoint of $\overline{X_1X_2}$ is taken as the origin O;
5. A line passing through O and perpendicular to X-axis is the Y-axis;
6. A line being $c_1\|X_1X_2\|$ far away from O and parallel to X-axis intersects the palm contour at passing O_1 and O_2;
7. A square region **S** of side length $c_2\|O_1O_2\|$, being symmetric with respect to Y-axis and $c_2\|O_1O_2\|$ far away from X-axis is extracted;
8. **S** is normalized to the size $N \times N$ and the result is taken as **R**.

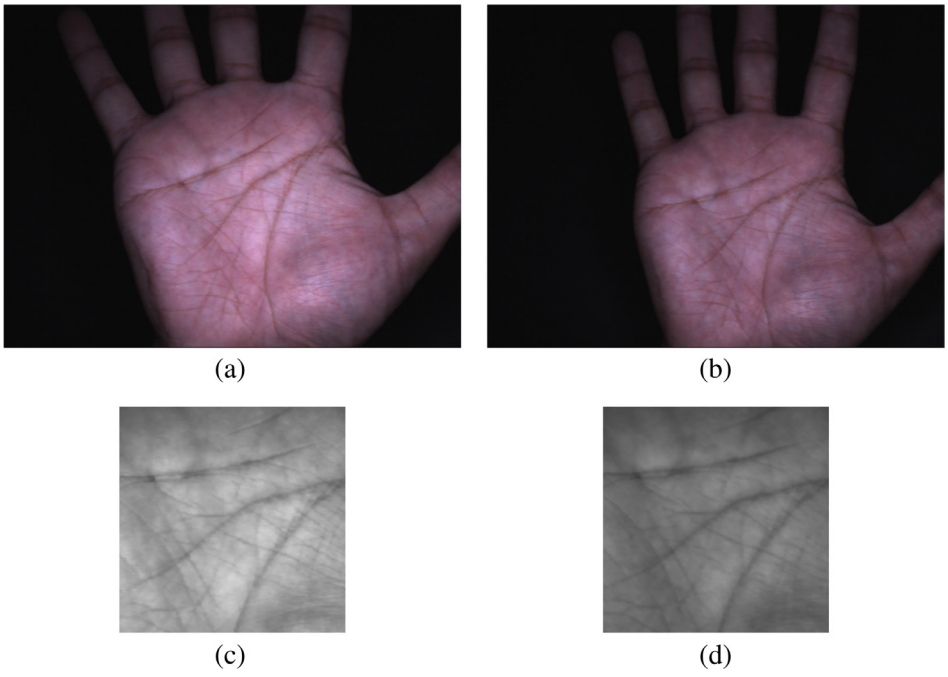

Fig. 6. (a) and (b) are two contactless palmprint images collected from the same palm in two different sessions while (c) and (d) are their ROIs, respectively.

is regarded as the origin O. Then, a line passing through O and perpendicular to X-axis is taken as the Y-axis. A line, which is $c_1\|X_1X_2\|$ far away from O and parallel to the X-axis can be determined. Suppose that this line intersects with the palm contour at O_1 and O_2. Then, a square region with the side length $c_2\|O_1O_2\|$, being symmetric with respect to the Y-axis and $c_3\|O_1O_2\|$ far way from the X-axis, is cropped. Finally, the cropped region is normalized to the size $N \times N$ and is regarded as the ROI. c_1, c_2, c_3, and N are some parameters and are empirically determined as $c_1 = 0.60$, $c_2 = 0.65$, $c_3 = 0.10$, and $N = 128$. The proposed ROI extraction scheme is illustrated inFig. 5 and its pipeline is summarized in Table 2. Two palmprint images and their corresponding ROIs are shown in Fig. 6. Fig. 6(a) and (b) are two images collected from the same palm but in different sessions and there is an apparent scale variation between them. However, from visual inspection, it can be seen that the two extracted ROIs are quite similar to each other, indicating that our ROI extraction algorithm is quite effective.

5. CR_CompCode: a novel approach for contactless palmprint identification

To solve the one-to-many identification problem, recent studies have found that the sparse representation based classification (SRC) [5] is an effective and efficient tool. Sparse representation codes a signal $\boldsymbol{y}$ over a dictionary $\mathbf{A}$ such that $\boldsymbol{y} \approx \mathbf{A}\boldsymbol{\alpha}$ and $\boldsymbol{\alpha}$ is a sparse coefficient vector. The sparsity of $\boldsymbol{\alpha}$ is measured by l_0-norm, counting the number of non-zero elements in $\boldsymbol{\alpha}$. Since the l_0-minimization is NP-hard, the l_1-minimization, as the closest convex function to l_0-minimization, is widely employed in sparse coding. However, in [49], Zhang et al. claimed that it is the collaborative representation (CR, i.e., using the gallery samples from all classes to represent the query sample $\boldsymbol{y}$) but not the l_1-norm sparsity that makes SRC powerful. Accordingly, they proposed to replace the l_1-norm sparsity regularization term in SRC framework with an l_2-norm regularization term and such a classification scheme is named as CRC_RLS (collaborative representation based classification with regularized least square). Zhang et al.'s experimental results on face datasets indicate that CRC_RLS could achieve comparable recognition accuracy as SRC; however, it runs much faster than SRC. The reason is that for CRC_RLS, there exists a simple closed-form solution while by contrast, solving SRC will involve a costly iterative optimization.

On seeing that CRC_RLS is a quite promising classification scheme, we propose to adapt it for contactless palmprint identification. To use CRC_RLS, how to extract feature vectors to represent palmprint images is a critical issue. Since there exits mere misalignment between two ROIs, the extracted feature vectors should be robust to small misalignment while still being highly discriminative. To meet these requirements, we propose a novel feature

extraction scheme for contactless palmprints based on block-wise statistics.

Given a palmprint ROI, we at first compute its CompCode map [38] by using a set of Gabor filters [50]. In the spatial domain, 2D Gabor filters can be expressed as:

$$G(x,y)=\exp\left(-\frac{1}{2}\left(\frac{x'^2}{\sigma_x^2}+\frac{y'^2}{\sigma_y^2}\right)\right)\exp\left(i2\pi fx'\right) \tag{1}$$

where $x'=x\cos\theta+y\sin\theta$ and $y'=-x\sin\theta+y\cos\theta$. In Eq. (1), f represents the frequency of the sinusoid wave, θ represents the orientation of the normal to the parallel stripes of the Gabor function, σ_x and σ_y are the standard deviations of the 2D Gaussian envelop. Denote by G_R the real part of a Gabor filter. With a bank of G_Rs sharing the same parameters, except the parameter for orientation, the local orientation information of the image I at the position (x, y) can be extracted and coded. Mathematically, this competitive coding process can be expressed as:

$$CompCode(x,y)=\arg\min_j\left(I(x,y)*G_R(x,y;\theta_j)\right) \tag{2}$$

where $*$ stands for the convolution operation, $\theta_j=j\pi/J$, $j=\{0,\ldots,J-1\}$, and J represents the number of orientations. We set $J=6$ in this paper and this is in accordance with the finding made by Lee [51] that the simple neural cells are sensitive to specific orientations with approximate bandwidths of $\pi/6$. Hence, each element of a CompCode map is an integer between $0\sim5$, representing the local dominant orientation.

CompCode maps are highly discriminative but they are sensitive to small amount of registration errors between the probe image and the training images. On the other hand, global statistics based features, such as histograms, are robust to misalignments but they are not quite discriminative. To combine the advantages of these two kinds of feature extraction ideas, we propose to use block-wise statistics of CompCode as features. Specifically, we uniformly partition the CompCode map into a set of $p\times p$ blocks. For each block i, we compute from it a histogram of CompCodes, denoted by $\boldsymbol{h}_i$. Obviously, the dimension of $\boldsymbol{h}_i$ is 6 since there are totally 6 possible CompCode values. Finally, all $\boldsymbol{h}_i$s are concatenated together as a large histogram $\boldsymbol{h}$, which is regarded as the feature vector.

With the proposed feature extraction scheme, given a contactless palmprint gallery set, we can compute a feature vector for each sample and then we define a dictionary matrix $\mathbf{A}$ for the entire gallery set as the concatenation of all the extracted feature vectors:

$$\mathbf{A}=[\boldsymbol{v}_{1,1},\boldsymbol{v}_{1,2},\ldots,\boldsymbol{v}_{k,n_k}]\in\mathcal{R}^{m\times n} \tag{3}$$

where k is the number of classes in the gallery set, n_k is the number of samples for class k, m is the dimension of features, and n is the total number of gallery samples. For robust classification, we require that $m<n$.

Given a probe palmprint image, denote by $\boldsymbol{y}\in\mathcal{R}^m$ its feature vector. Then $\boldsymbol{y}$ can be classified by the CRC_RLS model [49], which actually solves the following optimization problem:

$$\boldsymbol{x}_0=\arg\min_{\boldsymbol{x}}\left\{\|\boldsymbol{y}-\mathbf{A}\boldsymbol{x}\|_2^2+\lambda\|\boldsymbol{x}\|_2^2\right\} \tag{4}$$

where λ is a scalar weight. Eq. (4) has a closed-form solution as:

$$\boldsymbol{x}_0=\left(\mathbf{A}^T\mathbf{A}+\lambda\mathbf{I}\right)^{-1}\mathbf{A}^T\boldsymbol{y} \tag{5}$$

where $\mathbf{I}\in\mathcal{R}^{n\times n}$ is an identity matrix. Let $\mathbf{P}=\left(\mathbf{A}^T\mathbf{A}+\lambda\mathbf{I}\right)^{-1}\mathbf{A}^T$. Clearly, $\mathbf{P}$ is independent of $\boldsymbol{y}$ and can be pre-computed solely based on the gallery set. When $\boldsymbol{x}_0$ is available, we perform the classification by evaluating which class leads to the minimum representation error:

$$identity(\boldsymbol{y})=\arg\min_i\|\boldsymbol{y}-\mathbf{A}\delta_i(\boldsymbol{x}_0)\|_2^2 \tag{6}$$

Table 3
CR_CompCode: the algorithm for contactless palmprint identification.

Training phase
Input: A gallery set containing palmprint ROIs.
Output: The dictionary matrix $\mathbf{A}$.
1. For each sample j in the gallery set
   Extract from j a feature vector $\boldsymbol{v}_j$;
   Normalize $\boldsymbol{v}_j$ to make it have a unit l_2-norm;
2. Concatenate all $\boldsymbol{v}_j$s as $\mathbf{A}$.

Testing phase
Input: A query palmprint sample and $\mathbf{A}$.
Output: Class label of the query sample.
1. Extract the ROI from the query palmprint image.
2. Extract the feature vector $\boldsymbol{y}$ from the ROI.
3. Code $\boldsymbol{y}$ over $\mathbf{A}$ as
   $\boldsymbol{x}_0=\arg\min_{\boldsymbol{x}}\left\{\|\boldsymbol{y}-\mathbf{A}\boldsymbol{x}\|_2^2+\lambda\|\boldsymbol{x}\|_2^2\right\}$
4. Compute the residuals $r_i(\boldsymbol{y})=\|\boldsymbol{y}-\mathbf{A}\delta_i(\boldsymbol{x}_0)\|_2^2$.
5. $label(\boldsymbol{y})=\arg\min_i\{r_i(\boldsymbol{y})\}$.

Table 4
Benchmark contactless palmprint datasets.

Datasets	Number of palms	Number of sessions	Number of images
CASIA [34]	200	2	4800
IIT [35]	460	1	2601
GPDS100 [36]	100	1	1000
KTU [37]	145	1	1752
Our dataset	**600**	**2**	**12,000**

where $\delta_i(\boldsymbol{x}_0)$ is a new vector whose only nonzero entries are the entries in $\boldsymbol{x}_0$ that are associated with class i. Since our proposed palmprint identification approach uses the concatenation of local histograms of the CompCode map as the feature and the CR-based framework for classification, we name it as CR_CompCode for short. The pipeline of the algorithm CR_CompCode is summarized in Table 3 and its overall flowchart is demonstrated in Fig. 7.

6. Experiments

6.1. Newly established large-scale benchmark dataset

With the self-developed device, we have established a large-scale contactless palmprint image dataset. As our device is straightforward to use, the only instruction given to the subject is that he/she needs to stretch his/her hand naturally to make sure the finger gaps can be clearly observed on the screen. In our dataset, images were collected from 300 volunteers, including 192 males and 108 females. Those volunteers were staff or students of Tongji University. Among them, 235 subjects were $20\sim30$ years old and the others were $30\sim50$ years old. We collected samples in two separate sessions. In each session, the subject was asked to provide 10 images for each palm. Therefore, 40 images from 2 palms were collected from each subject. In total, the database contains 12,000 images captured from 600 different palms. The average time interval between the first and the second sessions was about 61 days. The maximum and minimum time intervals were 106 days and 21 days, respectively. The size of each image is 600×800. When you download the dataset, there are two folders, "session1" and "session2". "session1" contains images collected in the first session while "session2" comprises images collected in the second session. Two images in "session1" and "session2" having the same name were collected from the same palm. In each session, "00001 ~ 00010" were from the first palm, "00011 ~ 00020" were from the second palm, and so on. In each session, 6000 images were collected from 600 different palms.

Information about the publicly available datasets and our newly established one, in terms of the number of palms, the number of

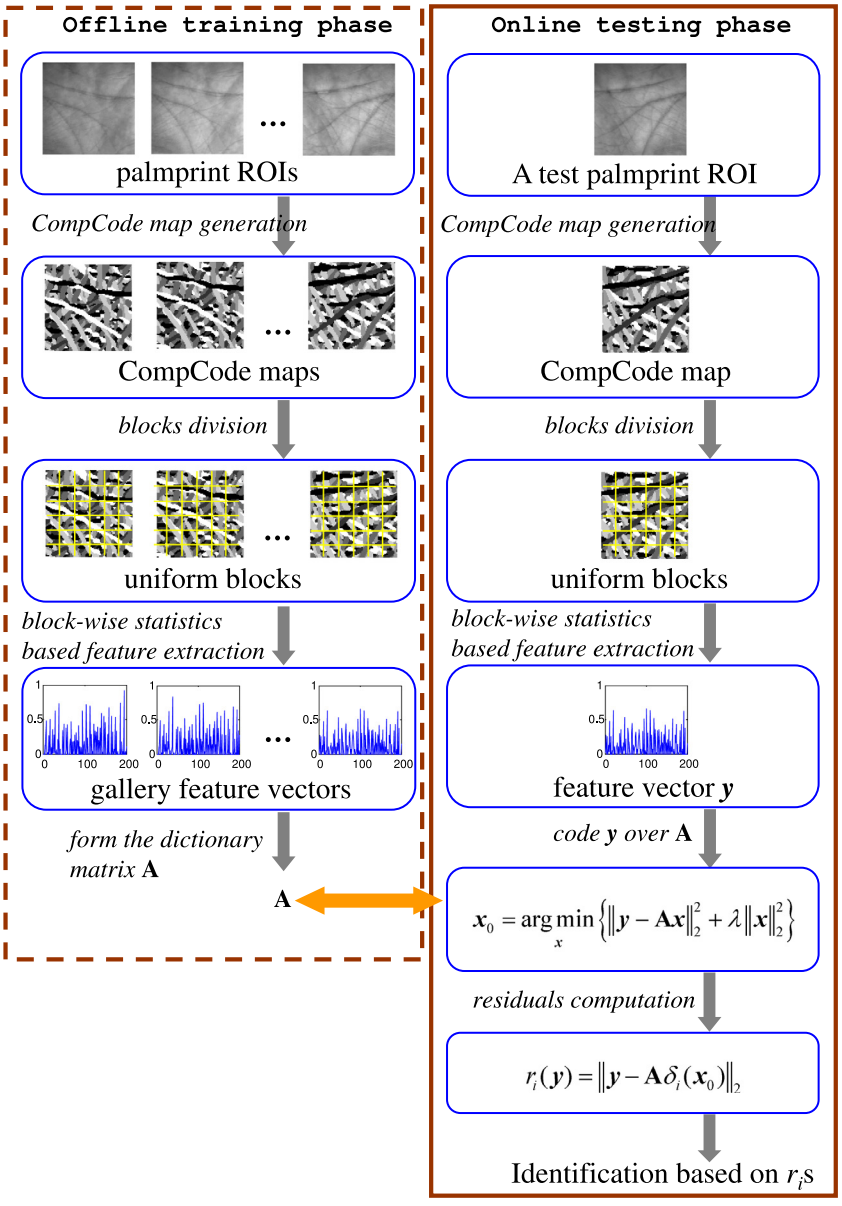

Fig. 7. Illustration for the proposed contactless palmprint identification scheme CR_CompCode.

collection sessions, and the total number of images, is summarized in Table 4. From Table 4, it can be seen that no matter which criterion is used, our dataset is the largest in scale. In addition, the image quality of our dataset is actually better than that of the existing ones (see Section 6.2 for more discussions about image quality). Hence, it can serve as a better benchmark for researchers to develop more advanced contactless palmprint recognition approaches.

6.2. Quality assessment of collected images

It is generally accepted that the quality of sample images has a significant impact on the performance of recognition methods. However, in the field of contactless palmprint recognition, no research has been conducted to quantify the quality of collected images objectively. In this experiment, we will evaluate the quality of images in benchmark datasets (CASIA [34], IIT [35], GPDS100 [36], KTU [37], and our dataset) from two aspects, the sharpness and the overall quality, using state-of-the-art IQA (image quality assessment) [52] models. Specifically, we randomly selected 200 images from each dataset and then extracted their ROIs. Each ROI was normalized to the size 256 × 256 and the quality assessment would be conducted on the normalized ROIs afterwards.

At first, it is generally accepted that a sharper image is more appealing for the recognition task since it may contain more discriminant visual features. That motivates us to use an objective metric to measure the sharpness of the acquired palmprint images. In this paper, the S_3 algorithm [53] is employed to perform this task since to the best of our knowledge it is a state-of-the-art method to automatically evaluate the sharpness of a given image. The S_3 index utilizes both spectral and spatial properties of the image. For each image block, it measures the slope of the magnitude spectrum and the total spatial variation. These measures are then combined via a weighted geometric mean to yield a perceived sharpness metric. A higher S_3 value indicates a higher perceptual sharpness.

In addition to the sharpness, we also care about the overall quality of palmprint images. In order to measure the palmprint image's overall quality, we resort to the IL-NIQE (Integrated Local Natural Image Quality Estimator) algorithm [54], which is a state-of-the-art approach in this field. IL-NIQE is a "completely blind"

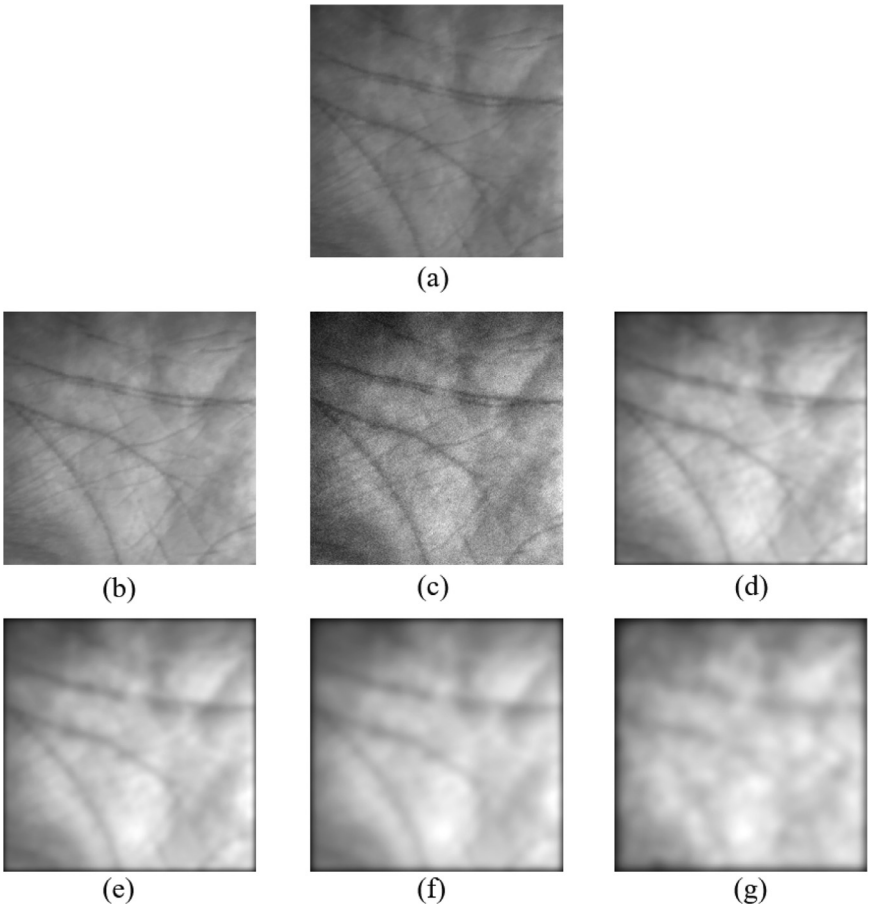

Fig. 8. (a) is the ROI of a palmprint image in the gallery set. (b) is the ROI of a test palmprint image. (a) and (b) belong to the same palm. (c) ~ (g) are quality-distorted versions of (b).

IQA model. It extracts various types of NSS (Natural Scene Statistics) features from a collection of pristine naturalistic images, and uses them to learn a multivariate Gaussian model of pristine images, which then serves as a reference model against which to predict the quality of the image patches. For a given test image, its patches are thus quality evaluated, then patch quality scores are averaged, yielding an overall quality score. A lower IL-NIQE value represents better image quality. Here we use an example to show that IL-NIQE is a good metric for objectively measuring the quality of a given palmprint image and that the image quality can really affect matching scores. Fig. 8(a) is the ROI of a palmprint image in the gallery set. Fig. 8(b) is the ROI of a test palmprint image. Fig. 8(a) and Fig. 8(b) actually belong to the same palm. We then simulated five quality-distorted versions of Fig. 8(b) and they are shown in Fig. 8(c) ~ (g). Measured by IL-NIQE, the quality indices of Fig. 8(b) ~ (g) are 88.08, 91.40, 112.12, 117.23, 127.23, and 130.68, respectively. It can be found that using IL-NIQE the quality evaluation results are highly consistent with human perception. We computed the matching distances between Fig. 8(a) and (b) ~ (g) with OLOF [40] and the resulting matching distances are 0.1915, 0.1925, 0.2229, 0.2306, 0.3077, and 0.3253, respectively. The relationship between the quality index and the matching distance can be more clearly observed through the plot shown in Fig. 9. It indicates that when the quality of the palmprint image degrades a lot, the matching error will be increased.

Using S_3 and IL-NIQE, the sharpness and the overall quality of images in benchmark datasets were evaluated and the obtained results are listed in Table 5. From Table 5, it can be seen that images in our dataset generally have higher sharpness and better overall quality. Thus, our dataset is more suitable to be employed to exploit the discriminant capability of the contactless palmprint.

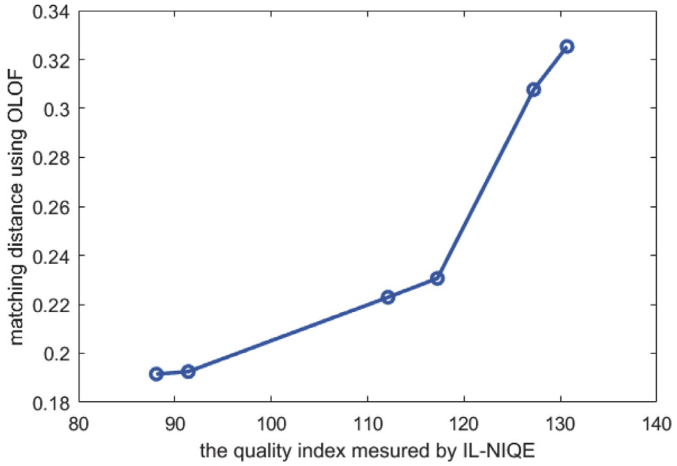

Fig. 9. The relationship between the quality index (measured by IL-NIQE) and the matching distance (measured by OLOF [40]).

6.3. Contactless palmprint identification

Identification experiments were conducted on our collected contactless palmprint dataset. We took samples collected in the first capturing session as the gallery set and samples collected in the second session as the probe set. With such an experimental

Table 5
Quality evaluation of images in benchmark contactless palmprint datasets.

	CASIA [34]	IIT [35]	GPDS100 [36]	KTU [37]	Ours
S_3 (Sharpness)	0.0560	0.0458	0.0387	0.0390	**0.0901**
IL-NIQE (Overall quality)	110.78	105.80	119.01	141.17	**101.32**

Table 6
Identification results on our contactless palmprint dataset.

	Recognition rate (%)	Time cost for 1 identification (ms)
PalmCode [30,41]	98.08	2665.41
OLOF [28,31]	98.82	2256.53
LBP+χ^2 [25]	94.08	478.15
SIFT+OLOF [43,44]	98.90	3901.79
SIFT+AlignedCompCode [45]	99.02	24,700.22
CR_CompCode	**98.78**	**12.48**

setting, the gallery set has 600 classes and for each class there are 10 samples. We use the rank-1 recognition rate as the performance measure. In addition, the running speed of each competing method was also evaluated. Experiments were performed on a workstation with an Intel i7-5960X CPU and 64G RAM. The software platform was Matlab2015a.

In order to demonstrate the superiority of CR_CompCode, several state-of-the-art matching methods in the field of contactless palmprint recognition were evaluated, including PalmCode [30,41] (originally proposed in [12]), OLOF [28,31] (originally proposed in [40]), LBP+χ^2-distance [25], SIFT+OLOF [43,44], and SIFT+AlignedCompCode [45].

For each identification method being evaluated, there are several parameters that need to be determined. For tuning parameters, we collected an extra small-scale palmprint dataset using the same device, which comprises 2000 images collected from 100 different palms. Images were collected in two separate sessions and in each session 10 images were collected for each palm. For each identification method, the parameters were empirically tuned in a greedy manner and the tuning criterion was that parameter values that could lead to a higher recognition rate would be chosen. As a result, key parameters used in CR_CompCode were set as follows, $\sigma_x = 4.85$ (see Eq. (1)), $\sigma_y = 9.31$ (see Eq. (1)), $f = 0.071$ (see Eq. (1)), $p = 14$ (the side length of the CompCode block), and $\lambda = 1.35$ (see Eq. (4)).

Experimental results are summarized in Table 6. In Table 6, we list the recognition rate achieved by each method. In addition, we also list the time cost consumed by one identification operation for each method. Given a test sample, the time cost for one identification operation includes the time consumed by the feature extraction and the time consumed by matching the test feature with the gallery feature set. In Fig. 10, the CMC (cumulative match characteristic) curves for all methods evaluated on our dataset are shown.

Based on the evaluation results listed in Table 6 and Fig. 10, we could have the following findings. With respect to the classification accuracy, the proposed method CR_CompCode could achieve comparable results with the state-of-the-art methods. Its rank-1 recognition rate is 98.78% on our benchmark dataset. Meanwhile, CR_CompCode runs greatly faster than all the other competing methods. For example, it is about 1979 times faster than SIFT+AlignedCompCode [45]. Under our experimental settings, it costs CR_CompCode only 12.48 ms to complete one identification operation against a gallery set comprising 6000 samples from 600 classes. The low speeds of the other methods evaluated can mainly be attributed to the brute-force matching strategy they adopt for identification. Take SIFT+AlignedCompCode [45] as an example. When it is used for identification, it needs to match the test sample to all the gallery samples and then figures out the most matched one. Meanwhile, when SIFT+AlignedCompCode matches a pair of palmprint samples, the following operations are conducted: SIFT matching, image alignment, CompCode extraction from the test sample, and CompCode matching. That explains the low speed of SIFT+AlignedCompCode for identification.

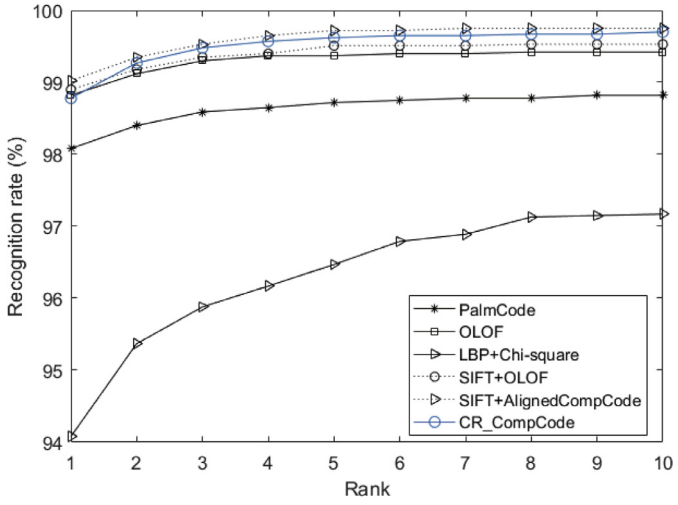

Fig. 10. CMC curves for all methods evaluated on our contactless palmprint dataset.

Based on above discussions, we recommend using the proposed CR_CompCode method for contactless palmprint identification since such an approach can achieve a distinguished high recognition accuracy while having an extremely low computational complexity. It is quite suitable for large-scale identification applications.

6.4. Computational complexity of CR_CompCode

In this section, we perform a computational complexity analysis for CR_CompCode. Denote the time cost for one multiplication operation by t_1, the time cost for one addition or subtraction operation by t_2, the time cost for one comparing operation by t_3, and the average number of samples for one class by c. The time cost for computing $\boldsymbol{x}_0$=$\mathbf{P}\boldsymbol{y}$ ($\mathbf{P} \in \mathcal{R}^{n\times m}$, $\boldsymbol{y} \in \mathcal{R}^{m\times 1}$) is $n(mt_1 + (m-1)t_2)$. The time cost for computing the residual for one class (see Eq. (6)) is $m(ct_1 + (c-1)t_2) + mt_2 + mt_1 + (m-1)t_2$. The time cost for identifying the minimum residual is $(k-1)t_3$. Thus, the total time cost for one identification operation by CR_CompCode is $(n + kc + k)mt_1 + (nm - n + kmc + km - k)t_2 + (k-1)t_3$.

6.5. About the identification certainty

When an identification system is deployed in practice, we need to consider the identification certainty issue. Given a test sample $\boldsymbol{t}$, its predicted class label is i. Then, we need to decide whether we can accept this identification result. For this purpose, we can check whether the reconstruction residual $r_i(\boldsymbol{t})$ lies within the confidence interval $[r_L, r_U]$ satisfying,

$$P(r_L < X < r_U) = 1 - \alpha \tag{7}$$

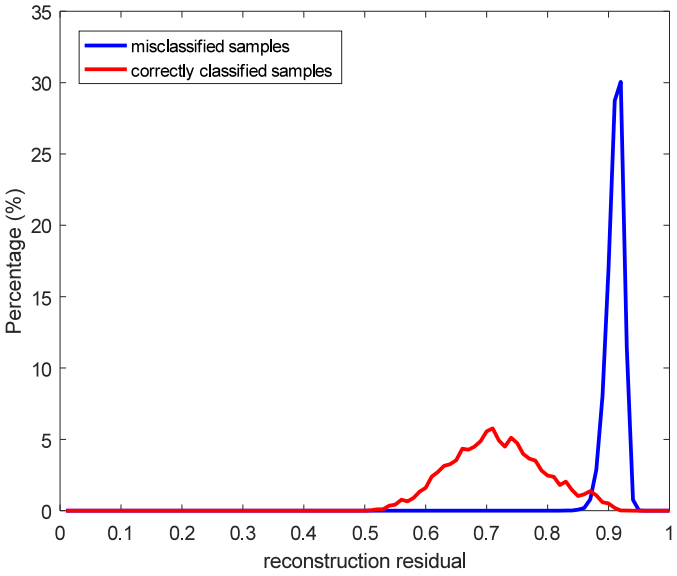

Fig. 11. Distributions of $\mathbb{R}_c$ (the set comprising reconstruction residuals of correctly classified samples) and $\mathbb{R}_w$ (the set comprising reconstruction residuals of misclassified samples).

where α is the confidence level. If $r_L < r_i(\boldsymbol{t}) < r_U$, the probability that the class label of $\boldsymbol{t}$ really is i is $1-\alpha$.

r_L and r_U can be empirically estimated. On our dataset, nearly all the test samples (98.78%) can be correctly classified. Thus, in order to enlarge the number of reconstruction residuals of misclassified samples, we also matched the palmprint images of the PolyU dataset [12] against our gallery set. As expected, each sample of the PolyU dataset was misclassified as one of the classes in our gallery set. Denote by $\mathbb{R}_c$ the set comprising reconstruction residuals of correctly classified samples and by $\mathbb{R}_w$ the set comprising reconstruction residuals of misclassified samples. Distributions of $\mathbb{R}_c$ and $\mathbb{R}_w$ are plotted in Fig. 11. With $\mathbb{R}_c$ and $\mathbb{R}_w$, r_L and r_U can be estimated straightforwardly. For example, in our case, if α is set as 0.05, $[r_L, r_U]$ is estimated as [0, 0.885].

7. Conclusions

In this work, we made an attempt towards exploring the discriminant capability of the contactless palmprint. To this end, we devised and developed a novel palmprint image acquisition device, which is highly user-friendly and can acquire high-quality palmprint images. Using the developed device, we collected a contactless palmprint image dataset comprising 12,000 samples collected from 600 different palms, which is larger in scale than all the existing benchmark datasets in this field. Moreover, the image quality of our dataset is better than that of other ones, which is corroborated by using two state-of-the-art blind IQA models. In addition, we proposed a novel method, namely CR_CompCode, for contactless palmprint identification. CR_CompCode can achieve a quite high recognition accuracy while having an extremely low computational complexity. On our dataset, CR_CompCode can complete one identification operation within 12.5 ms and its rank-1 recognition rate is 98.78%. Our system is suitable to be deployed to large-scale time-critical applications.

Acknowledgment

This work was supported in part by the Natural Science Foundation of China under grant no. 61672380 and in part by the ZTE Industry-Academia-Research Cooperation Funds under grant no. CON1608310007.

References

[1] A.K. Jain, P.J. Flynn, A. Ross, Handbook of Biometrics, Springer, 2007.
[2] D. Maltoni, D. Maio, A.K. Jain, S. Prabhakar, Handbook of Fingerprint Recognition, Springer, 2003.
[3] N. Ratha, B. Bolle, Automatic Fingerprint Recognition Systems, Springer, 2004.
[4] H. Wechsler, Reliable Face Recognition Methods-System Design, Implementation and Evaluation, Springer, 2006.
[5] J. Wright, A.Y. Yang, A. Ganesh, S.S. Sastry, Y. Ma, Robust face recognition via sparse representation, IEEE Trans. Pattern Anal. Mach. Intell. 31 (2) (2009) 210–227.
[6] Y. Taigman, M. Yang, M.A. Ranzato, L. Wolf, DeepFace: closing the gap to human-level performance in face verification, in: Proceedings of the IEEE International Conference on Computer Vision and Pattern Recognition, 2014, pp. 1701–1708.
[7] Y. Sun, X. Wang, X. Tang, Deeply learned face representations are sparse, selective, and robust, in: Proceedings of the IEEE International Conference on Computer Vision and Pattern Recognition, 2015, pp. 2892–2900.
[8] J.G. Daugman, High confidence visual recognition of persons by a test of statistical independence, IEEE Trans. Pattern Anal. Mach. Intell. 15 (11) (1993) 1148–1161.
[9] J. Daugman, How iris recognition works, IEEE Trans. Circuits Syst. Video Technol. 14 (1) (Jan. 2004) 21–30.
[10] K.W. Bowyer, K. Hollingsworth, P.J. Flynn, Image understanding for iris biometrics: a survey, Comput. Vision Image Understanding 110 (2) (May 2008) 281–307.
[11] J.K. Pillai, V.M. Patel, R. Chellappa, N.K. Ratha, Secure and robust iris recognition using random projections and sparse representations, IEEE Trans. Pattern Anal. Mach. Intell. 33 (9) (2011) 1877–1893.
[12] D. Zhang, W. Kong, J. You, M. Wong, Online palmprint identification, IEEE Trans. Pattern Anal. Mach. Intell. 25 (9) (Sep. 2003) 1041–1050.
[13] A.K. Jain, J. Feng, Latent palmprint matching, IEEE Trans. Pattern Anal. Mach. Intell. 31 (6) (Jun. 2009) 1032–1047.
[14] L. Zhang, H. Li, Encoding local image patterns using Riesz transforms: with applications to palmprint and finger-knuckle-print recognition, Image Vision Comput. 30 (12) (Oct. 2012) 1043–1051.
[15] L. Zhang, Y. Shen, H. Li, J. Lu, 3D palmprint identification using block-wise features and collaborative representation, IEEE Trans. Pattern Anal. Mach. Intell. 37 (8) (Aug. 2015) 1730–1736.
[16] D. Zhang, G. Lu, 3D Biometrics–Systems and Applications, Springer, 2013.
[17] R. Sanchez-Reillo, C. Sanchez-Avila, A. Gonzalez-Marcos, Biometric identification through hand geometry measurements, IEEE Trans. Pattern Anal. Mach. Intell. 22 (10) (Oct. 2000) 1168–1171.
[18] L. Zhang, L. Zhang, D. Zhang, H. Zhu, Online finger-knukle-print verification for personal authentication, Pattern Recognit. 43 (7) (2010a) 2560–2571.
[19] L. Zhang, L. Zhang, D. Zhang, Z. Guo, Phase congruency induced local features for finger-knukle-print recognition, Pattern Recognit. 45 (7) (2012b) 2522–2531.
[20] G. Gao, L. Zhang, J. Yang, L. Zhang, D. Zhang, Reconstruction based finger-knuckle-print verification with score level adaptive binary fusion, IEEE Trans. Image Process. 22 (12) (Dec. 2013) 5050–5062.
[21] L. Zhang, L. Li, H. Li, M. Yang, 3D ear identification using block-wise statistics based features and LC-KSVD, IEEE Trans. Multimedia 18 (8) (Aug. 2016) 1531–1541.
[22] H. Cummins, M. Midlo, Finger Prints, Palms and Soles: An Introduction to Dermatoglyphics, Dover Publications, 1961.
[23] X. Wu, Q. Zhao, W. Bu, A SIFT-based contactless palmprint verification approach using iterative RANSAC and local palmprint descriptors, Pattern Recognit. 47 (10) (Oct. 2014) 3314–3326.
[24] V. Kanhangad, A. Kumar, D. Zhang, A unified framework for contactless hand verification, IEEE Trans. Inf. Forensics Secur. 6 (3) (Oct. 2011) 1014–1027.
[25] G.K.O. Michael, T. Connie, A.B.J. Teoh, Touch-less palm print biometrics: novel design and implementation, Image Vision Comput. 26 (12) (Dec. 2008) 1551–1560.
[26] W. Chen, Y. Chiang, Y. Chiu, Biometric verification by fusing hand geometry and palmprint, in: Proceedings of the International Conference on Intelligent Information Hiding and Multimedia Signal Processing, 2007, pp. 403–406.
[27] A. Kumar, Incorporating cohort information for reliable palmprint authentication, in: Proceedings of the Indian Conference on Computer Vision, Graphics and Image Processing, 2008, pp. 583–590.
[28] Y. Hao, Z. Sun, T. Tan, C. Ren, Multispectral palm image fusion for accurate contact-free palmprint recognition, in: Proceedings of the IEEE International Conference on Image Processing, 2008, pp. 281–284.
[29] G.K.O. Michael, T. Connie, A.T.B. Jin, An innovative contactless palm print and knuckle print recognition system, Pattern Recognit. Lett. 31 (12) (Sep. 2010) 1708–1719.
[30] A. Poinsot, F. Yang, M. Paindavoine, Small sample biometric recognition based on palmprint and face fusion, in: Proceedings of the International Multi-Conference on Computing in the Global Information Technology, 2009, pp. 118–122.
[31] M. Ferrer, F. Vargas, A. Morales, BiSpectral contactless hand based biometric system, in: Proceedings of the National Conference on Telecommunications, 2011, pp. 1–6.
[32] A. Morales, M.A. Ferrer, C.M. Travieso, J.B. Alonso, Multisampling approach applied to contactless hand biometrics, in: Proceedings of the IEEE International Carnahan Conference on Security Technology, 2012, pp. 224–229.

[33] M. Aykut, M. Ekinci, Developing a contactless palmprint authentication system by introducing a novel ROI extraction method, Image Vision Comput. 40 (Aug. 2015) 65–74.
[34] CASIA multi-spectral palmprint database, [Online]. Available: http://biometrics.idealtest.org/dbDetailForUser.do?id=6.
[35] IIT Delhi touchless palmprint database, [Online]. Available: http://www4.comp.polyu.edu.hk/~csajaykr/IITD/Database_Palm.htm.
[36] GPDS100 contactless hands 2Band database, [Online]. Available: http://www.gpds.ulpgc.es/download/.
[37] KTU contactless palmprint database, [Online]. Available: http://ceng2.ktu.edu.tr/~cvpr/contactlessPalmDB.htm.
[38] A. Kong, D. Zhang, Competitive coding scheme for palmprint verification, in: Proceedings of the IEEE International Conference on Pattern Recognition, 2004, pp. 520–523.
[39] W. Jia, D. Huang, D. Zhang, Palmprint verification based on robust line orientation code, Pattern Recognit. 41 (5) (May 2008) 1504–1513.
[40] Z. Sun, T. Tan, Y. Wang, S.Z. Li, Ordinal palmprint representation for personal identification, in: Proceedings of the IEEE InternationalConference on Computer Vision and Pattern Recognition, 2005, pp. 279–284.
[41] J. Doublet, O. Lepetit, M. Revenu, Contact less hand recognition using shape and texture features, in: Proceedings of the IEEE International Conference on Signal Processing, 2006, pp. 1–6.
[42] D.G. Lowe, Distinctive image features from scale-invariant keypoints, Int. J. Comput. Vision 60 (2) (Nov. 2004) 91–110.
[43] A. Morales, M.A. Ferrer, A. Kumar, Improved palmprint authentication using contactless imaging, in: Proceedings of the IEEE International Conference on Biometrics: Theory Applications and Systems, 2010, pp. 1–6.
[44] A. Morales, M.A. Ferrer, A. Kumar, Towards contactless palmprint authentication, IET Comput. Vision 5 (6) (Nov. 2011) 407–416.
[45] Q. Zhao, W. Bu, X. Wu, SIFT-based image alignment for contactless palmprint verification, in: Proceedings of the IEEE International Conference on Biometrics, 2013, pp. 1–6.
[46] X. Wu, Q. Zhao, Deformed palmprint matching based on stable regions, IEEE Trans. Image Process. 24 (12) (Dec. 2015) 4978–4989.
[47] M. Ekinci, M. Aykut, Kernel Fisher discriminant analysis of Gabor features for online palmprint verification, Turk. J. Electr. Eng. Comput. Sci. 24 (2) (Jan. 2016) 355–369.
[48] S. Mika, G. Ratsch, J. Weston, B. Scholkopf, K.R. Millers, Fisher discriminant analysis with kernels, in: IEEE Signal Processing Society Workshop, 1999, pp. 41–48.
[49] L. Zhang, M. Yang, X. Feng, Sparse representation or collaborative representation: which helps face recognition? in: Proceedings of the IEEE International Conference on Computer Vision, 2011, pp. 471–478.
[50] J.G. Daugman, Uncertainty relation for resolution in space, spatial frequency, and orientation optimized by two-dimensional visual cortical filters, J. Opt. Soc. Am. A 2 (7) (Jul. 1985) 1160–1169.
[51] T. Lee, Image representation using 2D Gabor wavelet, IEEE Trans. Pattern Anal. Mach. Intell. 18 (10) (Oct. 1996) 957–971.
[52] Z. Wang, A.C. Bovik, Modern Image Quality Assessment, Morgan & Claypool, San Rafael, CA, USA, 2006.
[53] C.T. Vu, T.D. Phan, D.M. Chandler, S3: a spectral and spatial measure of local perceived sharpness in natural images, IEEE Trans. Image Process. 21 (3) (Mar. 2012) 934–945.
[54] L. Zhang, L. Zhang, A.C. Bovik, A feature-enriched completely blind image quality evaluator, IEEE Trans. Image Process. 24 (8) (Aug. 2015) 2579–2591.

Lin Zhang received the B.Sc. and M.Sc. degrees from the Department of Computer Science and Engineering, Shanghai Jiao Tong University, Shanghai, China, in 2003 and 2006, respectively. He received the Ph.D. degree from the Department of Computing, the Hong Kong Polytechnic University, Hong Kong, in 2011. From March 2011 to August 2011, he was a Research Assistant with the Department of Computing, the Hong Kong Polytechnic University. In Aug. 2011, he joined the School of Software Engineering, Tongji University, Shanghai, China, where he is currently an Associate Professor. His current research interests include biometrics, pattern recognition, computer vision, and perceptual image/video quality assessment.

Lida Li received the B.S. and M.Sc. degrees from the School of Software Engineering, Tongji University, Shanghai, China, in 2013 and 2016, respectively. He is now pursuing his Ph.D. degree at the department of Computing, The Hong Kong Polytechnic University, Hong Kong. His research interests are biometrics and machine learning.

Anqi Yang is now pursuing her B.Sc. degree at the School of Software Engineering, Tongji University, Shanghai, China. His research interests include computer vision and machine learning.

Ying Shen received the B.S. and M.S. degrees from the Software School, Shanghai Jiao Tong University, Shanghai, China, in 2006 and 2009, respectively. She received the Ph.D. degree from the Department of Computer Science, City University of Hong Kong, Hong Kong, in 2012. In 2013, she joined the School of Software Engineering, Tongji University, Shanghai, China, and currently is an assistant professor. Her research interests include machine learning and pattern recognition.

Meng Yang is currently an associate professor at School of Computer Science and Software Engineering, Shenzhen University, Shenzhen, China. He received his Ph.D. degree from The Hong Kong Polytechnic University in 2012. Before joining Shenzhen University, he has been working as Postdoctoral fellow in the Computer Vision Lab of ETH Zurich. His research interest includes sparse coding, dictionary learning, object recognition and machine learning. He has published 9 AAAI/CVPR/ICCV/ECCV papers and several IJCV, IEEE TNNLS and TIP journal papers.